A numerical study on convergence of alongshore flows over the Texas-Louisiana shelf

Zhaoru Zhang[1,2] and Robert Hetland[1]

Received 18 April 2012; revised 13 September 2012; accepted 21 September 2012; published 9 November 2012.

[1] A hydrodynamic model is used to investigate convergent alongshore flows over the Texas-Louisiana shelf, characterized by down-coast flows over the northern shelf encountering up-coast flows over the southern shelf. The model's ability to reproduce realistic current, salinity, and surface elevation fields is demonstrated through positive model skill scores when comparing model simulations to observational data. The convergent flows are explored on both weather band and seasonal time scales. For weather band scales, this study focuses on wintertime convergent events. The model-predicted locations of convergent flows are supported by current measurements. We find that the formation of convergent flows is primarily caused by along-coast variation in the alongshore component of wind forcing, which in turn is due to the curvature of the Texas-Louisiana coastline. In general, the alongshore currents are well correlated with alongshore winds. However, the convergence points of currents and winds are not colocated, but rather, convergence points in ocean currents typically occur down coast of convergence points in the wind. This offset is demonstrated to be mainly caused by buoyancy forcing that can drive the convergence location in the currents farther down coast. No specific temporal pattern is found for the weather band convergence locations, whereas at seasonal time scales, the monthly mean convergence exhibits a prominent seasonal pattern, with up-coast migration of convergence locations in spring and summer and down-coast migration in fall and winter.

Citation: Zhang, Z., and R. Hetland (2012), A numerical study on convergence of alongshore flows over the Texas-Louisiana shelf, *J. Geophys. Res.*, *117*, C11010, doi:10.1029/2012JC008145.

1. Introduction

[2] The Texas-Louisiana shelf is located in the northwestern Gulf of Mexico, and is an economically important coastal region due to extensive offshore oil and gas activities, commercial and sport fishing, and coastal tourism. These activities are all significantly affected by shelf dynamics. A prominent dynamical feature over this shelf is convergence (or called confluence in some studies) in the alongshore coastal flows, which is characterized by down-coast (in the sense of Kelvin wave propagation, i.e., from Louisiana to Texas) flow along the northern section of the coast encountering up-coast flow along the southern section of the coast. Convergent flows can concentrate floating material near the coast, and are thus important in understanding and predicting shoreline impacts of oil spills, as well as in harmful algae bloom initiation and subsequent transport [*Hetland and Campbell*, 2007]. However, up until now, the convergent flows have only been briefly discussed in previous studies, and the factors controlling this phenomenon have not yet been well studied. This paper aims to provide a deeper insight into the processes that control convergent flow patterns, and their temporal variation.

[3] To understand the convergence phenomenon, it is important to know the dynamical background of the Texas-Louisiana shelf. Previous studies have demonstrated that seasonal circulation over the inner shelf (inshore of the 50 m isobath) is primarily modulated by alongshore winds. Alongshore winds and currents both show a pattern of annual reversal. In nonsummer months (September through May) the prevailing down-coast winds drive down-coast flows; in summer months (May to August) the prevailing winds shift to upwelling favorable and drive up-coast flows [*Cochrane and Kelly*, 1986; *Cho et al.*, 1998]. Buoyancy fluxes from the Mississippi-Atchafalaya river discharge are known to affect circulation patterns and alter salinity distributions as far south as the Texas-Mexico border [*Morey et al.*, 2005; *Zavala-Hidalgo et al.*, 2003]. Offshore Loop Current Eddies are another major forcing mechanism of the circulation, and the outer shelf circulation is frequently affected by offshore eddies [*Li et al.*, 1996; *Nowlin et al.*, 2005; *Oey*, 1995]. Over the weather band (2–10 days), the shelf circulation is largely influenced by frontal passages, cold air mass outbreaks,

[1]Department of Oceanography, Texas A&M University, College Station, Texas, USA.
[2]Physical Oceanography Laboratory, Ocean University of China, Qingdao, China.

Corresponding author: Z. Zhang, Department of Oceanography, Texas A&M University, 3146 TAMU, College Station, TX 77843-3146, USA. (zhaoruzhang@gmail.com)

cyclogenesis and hurricanes [*Nowlin et al.*, 1998a, 1998b]. A prominent high-frequency phenomenon over the shelf is near-inertial oscillations, which are driven by diurnal winds and characterized by clockwise-rotating currents with frequencies slightly higher than the local inertial frequency [*Zhang et al.*, 2009, 2010]. Since our focus is on the convergent flows near the coastline, subinertial alongshore wind and riverine buoyancy fluxes are expected be the two primary factors controlling the phenomenon.

[4] Convergent flows have been observed in several studies of the Texas-Louisiana shelf dynamics. They were first noted in the 1950s through ship's drift information [*Leipper*, 1954] and their existence was further supported in the 1970s by drift bottle studies [*Watson and Brehens*, 1970; *Hunter et al.*, 1974]. *Cochrane and Kelly* [1986] first explained the occurrence of convergent currents with a conceptual model: with uniform wind stress blowing toward the coast of the northwestern Gulf, the curvature of the coastline creates a change in direction of the alongshore wind stress. Since alongshore currents typically flow in the direction of the alongshore wind stress, the convergence of alongshore wind creates a convergence in alongshore current. *Morey et al.* [2005] and *Zavala-Hidalgo et al.* [2003] found convergent flows in the western Gulf of Mexico based on numerical simulations forced with monthly mean winds. They also suggested that convergent flows occur as a result of a change in the sign of alongshore wind caused by the bending of the coastline. According to their studies, the convergence of monthly mean current migrates up coast with the convergence of alongshore wind from winter to summer. In the convergence region transport of coastal water offshore is enhanced. Convergence phenomena have also been noted on other continental shelves. For example, *Yuan et al.* [2005] suggested that cross-shelf penetrating fronts observed off the southeast coast of China might be associated with the convergence of two current systems flowing in opposing directions.

[5] All of the previous studies on the Texas-Louisiana shelf convergent flows focused on seasonal time scales. However, there is a substantial need to understand these flows at much shorter time scales. Oil spill and harmful algal bloom trajectory prediction requires predicting flow on time scales of days. Therefore, this study will focus more on the weather band convergence that has not been discussed before, while seasonal convergence is also included as an extension of previous work. Also, previous studies only analyzed the relationship between convergent flows and local wind forcing; other factors affecting the shelf currents, such as buoyancy forcing, were not considered. Buoyancy effects are shown below to influence convergence locations.

[6] It is difficult to study convergent flows using existing observations on the Texas-Louisiana shelf due to the fact that these observations do not have either sufficient spatial or temporal resolution to resolve the locations of convergence. Therefore, we believe a numerical simulation is the most appropriate tool for this investigation.

2. Model

2.1. Model Setup

[7] The model employed here is the Regional Ocean Modeling System (ROMS). ROMS is a free-surface, terrain-following hydrodynamic and primitive equations ocean model widely used in regional oceanic studies [*Shchepetkin and McWilliams*, 2005]. The model grid covers the entire Gulf of Mexico with uneven horizontal grid spacing. The highest resolution is in the northwestern section of the Gulf with grid spacing of 4 km; in the southeastern Gulf the resolution is relatively coarse and approximately 15 km (Figure 1). The model has 10 vertical layers. The northern and western boundaries are closed with no-slip boundary conditions, while the southern and eastern boundaries are opened at the Yucatan Channel and the Florida Straits, respectively. The model does not attempt to reproduce the Loop Current system by inducing a western boundary current flow through the Yucatan Channel and the Florida Straits. However, as shown below in the model-data comparison, the wind and river forcing are the dominant forcing mechanisms driving currents inshore of 30 m, the primary focus region of this study.

[8] The model is initialized on 1 January 2000 with zero velocity and climatological profiles for temperature and salinity based on historical hydrographic surveys. At the open boundaries, a Chapman condition [*Chapman*, 1985] is used for surface elevation and a Flather condition [*Flather*, 1976] is used for 2-D momentum equations. Radiation conditions are used for 3-D momentum equations and tracers. Near the open boundaries, climatological nudging is applied to tracers and 3-D velocities. Temperature and salinity are nudged to horizontally uniform monthly climatological values and 3-D velocities are nudged to zero values to suppress the development of instability eddies. The nudging time scale for both tracers and velocities is 1 day at the outermost layer and increases toward the inner layers.

[9] Atmospheric forcing for the model includes 3-hourly surface wind speed, shortwave radiation, air temperature, air pressure, relative humidity, cloud and precipitation from the North American Regional Reanalysis (NARR) data set. Longwave radiation is computed internally within ROMS. The model is forced by fresh water discharge from the Mississippi and Atchafalaya rivers based on daily measurements at Tarbert Landing conducted by the U.S. Army Corps of Engineers. The total integration time of the model is 11 years. In this research, the simulation with a configuration described above is referred to as the reference run, and most of the subsequent analysis is based on the reference run. To investigate the effect of buoyancy forcing on the formation of convergent flows, a control run that has the river forcing taken out is also performed. The other aspects of the configuration for the control run are exactly the same as in the reference run.

2.2. Model Assessment

2.2.1. Surface Current Simulations

[10] The performance of the model in reproducing observed current, salinity and surface elevation fields is evaluated against observational data. The simulated surface currents are compared with buoy measurements provided by the Texas Automated Buoy System (TABS, http://tabs.gerg.tamu.edu/). TABS is a coastal network of moored buoys that report near real-time observations of surface currents and winds along the Texas coast. Currently, it consists of nine active sites, seven along the Texas coast and two offshore (Figure 1). Figure 2 shows the comparison between the

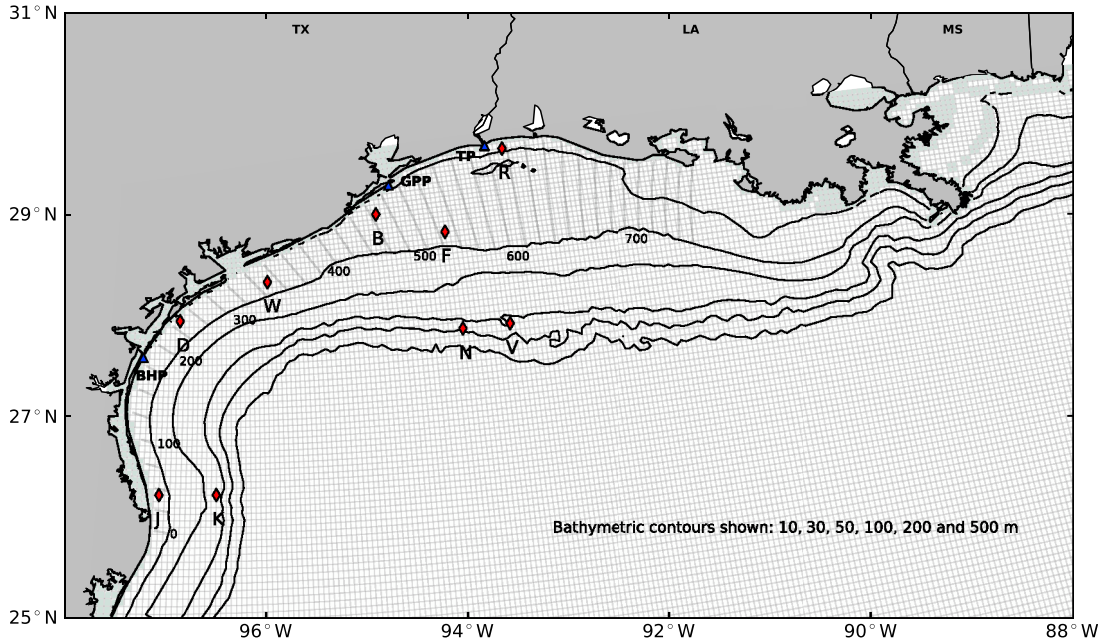

Figure 1. A map of the Texas-Louisiana shelf shown with the numerical grid superimposed. The bathymetric contours are shown for the 10, 30, 50, 100, 200, and 500 m isobaths. A subset of the model grid is included to show the model resolution (light gray squares); the filled light green squares mark the land mask of the model. The TABS buoy sites are marked with red diamonds, and the TCOON stations (Bob Hall Pier (BHP), Galveston Pleasure Pier (GPP), and Texas Point (TP)) are marked with blue triangles. Also plotted are the cross-shore transects from the south Texas coast to the central Louisiana coast, which will be used in subsequent analysis, and the along-coast distance (in kilometers) of these transects to the origin (the southernmost transect) is labeled at a 100 km interval. In this paper, a transect is noted by its location, e.g., the 100 km transect refers to the transect at a distance of 100 km from the origin.

modeled and observed surface alongshore velocities at the TABS buoy sites for year 2006. Model skill and the correlation coefficient between modeled and observed values are provided for each buoy. The model skill is defined as

$$skill = 1 - \frac{\sum_{i=1}^{i=N} (d_i - \mathcal{L}[m_i])^2}{\sum_{i=1}^{i=N} (d_i - c_i)^2}, \quad (1)$$

where d_i are observations, m_i are model results that are converted to observational space by a linear operator $\mathcal{L}$, c_i are climatological values, and N is the number of total observations [*Hetland*, 2006]. In this study, the climatological values are computed from the buoy data and defined as monthly mean values averaged over year 2000 through 2009. From equation 1, if the variance of the model error (the numerator in the summation) is smaller than the variance of observations (the determinator) at a buoy location, then the model skill is positive.

[11] Figure 2 shows that for most buoys, the model is able to capture the variability of the observed alongshore surface currents on seasonal time scales as well as on the weather band. Positive model skill indicates that the model is a more accurate representation of observations than climatology. The nearshore buoys, such as buoys B, D, J, R and W, all have relatively higher model skill because the alongshore flows near the coast are primarily driven by winds. On the other hand, the offshore buoys, such as buoy K, N and V, have negative or very low model skill as a result of the influence of offshore eddies, which are not represented in the current model setup; this model does not contain a Loop Current or Loop Current Eddies. For the inner-shore buoys, the coherence between modeled and observed alongshore currents is generally high (between 0.7 and 0.8) for the seasonal scale, while for the weather band there is more variability in the coherence. However, power spectra (not shown) for simulated and observed currents are similar for the weather band and lower-frequency variability, with discrepancies well within the error of the spectra. This indicates that the model is able to capture the magnitude of the variability of currents in the weather band.

2.2.2. Salinity Field Assessment

[12] Two independent data sets are used for evaluating the model salinity field. The first one is from the Southeast Area Monitoring and Assessment Program (SEAMAP). Its component in the Gulf of Mexico regularly collects fishery and environmental data, including temperature and salinity vertical profiles along the Texas-Louisiana continental shelf (M. Marta-Almeida et al., Evaluation of model nesting performance on the Texas-Louisiana continental shelf, manuscript in preparation, 2012). In this study, we use the SEAMAP salinity data collected during May, June, and July of 2005 through 2008. This includes 1003 measurement profiles. For the model skill assessment (Figure 3), only data

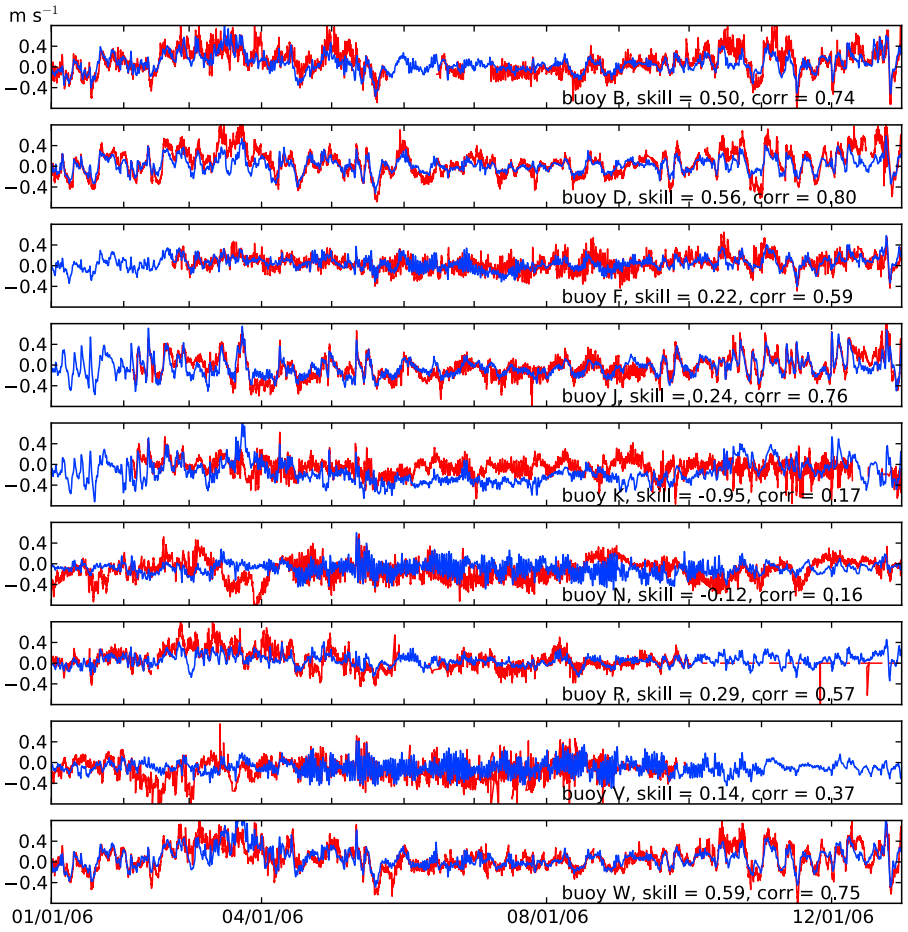

Figure 2. Comparison of surface alongshore currents between the model simulations (blue lines) and TABS buoy measurements (red lines) for the year 2006. The values of model skill and correlation are provided.

in the upper 50 m of water column are used, and the error presented for each profile is the vertically averaged value normalized by the standard deviation of data on this profile. The climatological data used here and for the second data set are the same as those used in *Hetland and DiMarco* [2011]. Figure 3 shows that model skills are positive for all the separate SEAMAP data collection periods, and on the whole the model skill exceeds 0.5 (Figure 3, bottom right).

[13] The second data set used for assessment is from the Mechanisms Controlling Hypoxia (MCH) project. MCH collected vertical profiles of salinity, temperature and dissolved oxygen concentration data from March to August for year 2004 through 2008 except 2006 [*DiMarco et al.*, 2010; *Zhang et al.*, 2012a]. A total of 1346 profiles are employed in our model-data comparison, as shown in Figure 4, and again, only salinity data in the upper 50 m of the water column are used for computing model errors and skills. For most of the MCH measurement periods the model skill is higher than 0.5, and the highest value is 0.78.

[14] Therefore, we conclude that the model is able to simulate the observed salinity field reasonably well. Thus, we expect that the model is able to produce realistic, broad-scale buoyancy forcing over the shelf associated with the Mississippi/Atchafalaya river plume system. This is important, since we demonstrate below that buoyancy forcing influences the locations of the confluence regions.

2.2.3. Surface Elevation Simulations

[15] The model surface elevation simulations are evaluated against measurements from the Texas Coastal Ocean Observation Network (TCOON, http://lighthouse.tamucc.edu/TCOON/HomePage). We compared observational and modeled surface elevations referenced to their annual mean values at three TCOON stations that are not inside a bay (Bob Hall Pier, Galveston Pleasure Pier and Texas Point, Figure 1) for year 2008 (this year has almost complete data coverage). Results (not shown) indicate that the variability of observational elevation is well captured by the model simulation for all the three stations, with positive model skills between 0.46 and 0.65.

3. Results

[16] Alongshore currents over the Texas-Louisiana shelf undergo a reversal from nonsummer to summer months, and the occurrence of convergent flows changes accordingly. In this section, when analyzing the seasonal patterns of convergence, we include both the winter and summer flow regimes. However, for weather band time scales we mostly

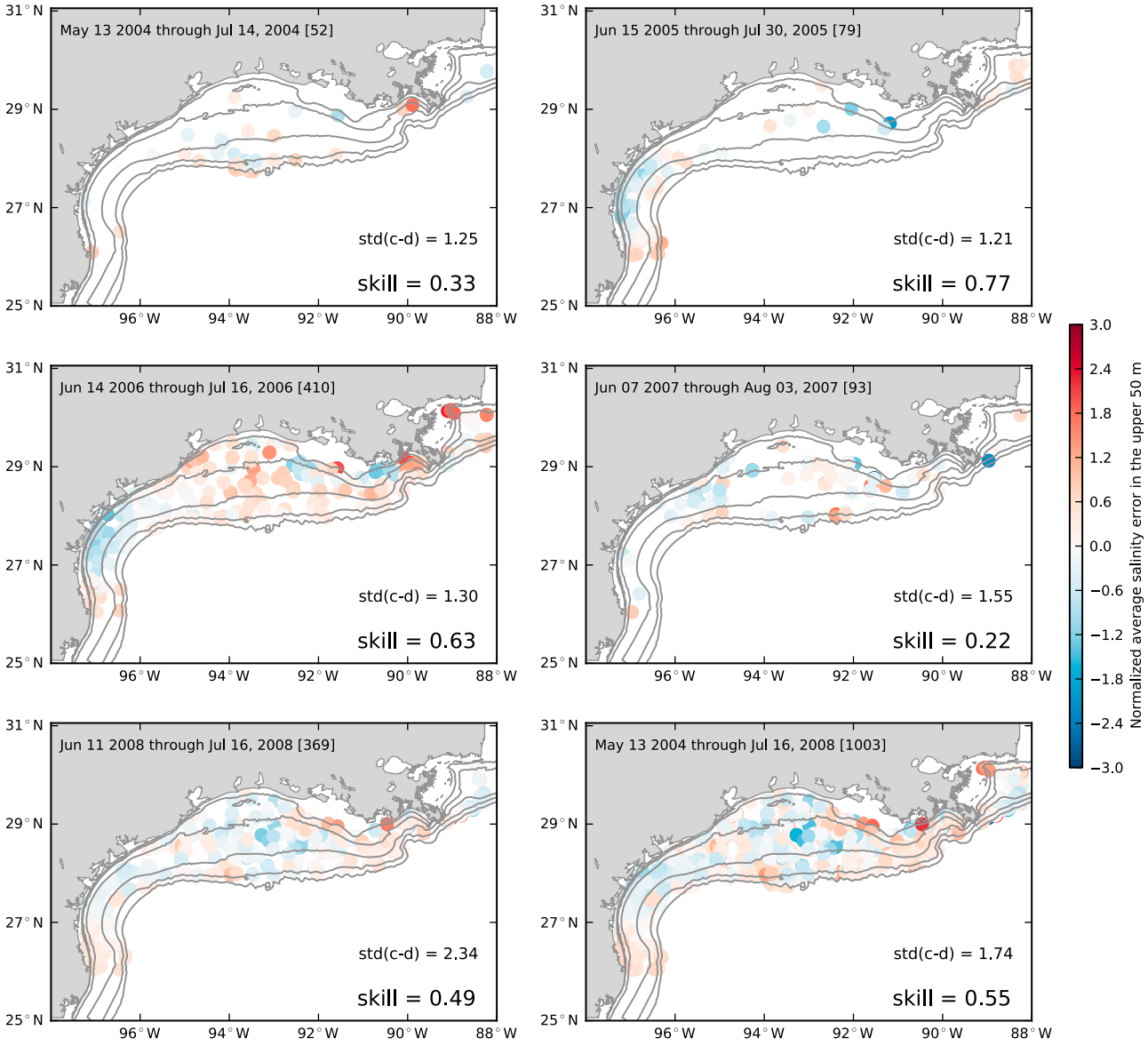

Figure 3. Errors between the model simulated salinity and the SEAMAP measurements averaged over the upper 50 m of water column and normalized by the standard deviation of the difference between the SEAMAP measurements and climatological values for five SEAMAP data collection periods show the spatial patterns of model error for this set of hydrographic measurements. The bottom right panel shows the statistics for all data collected during these periods. The standard deviation of the difference between the observed and climatological values and model skill are provided for each panel.

focus on the winter regime due to the fact that coastal flows in summertime are much weaker and less organized because of weaker wind forcing and stronger vertical stratification [*Cho et al.*, 1998; *Jarosz and Murray*, 2005]. Thus, it is more difficult to distinguish convergence events in summer. Model results for year 2006 are used in subsequent analyses since this year shows, overall, better agreement between the simulation and observations, and thus should be a more faithful reproduction of the actual flow field. Winds and currents are both subject to a 33 h low-band-pass filter to remove near-inertial and higher-frequency motions.

3.1. Simulated Surface Convergent Flows on Weather Band

[17] Figure 5 shows four snapshots of surface flow fields over the Texas-Louisiana shelf when convergent alongshore currents are observed in February 2006, i.e., during non-summer, with surface wind and salinity fields superimposed. From these four examples and other convergent events observed in our simulations, we find that convergence mostly occurs near the coast located between Galveston Bay (29.3°N, 94.8°W) and Baffin Bay (27.2°N, 97.5°W) of Texas. This is the transition zone of the shelf from the north-

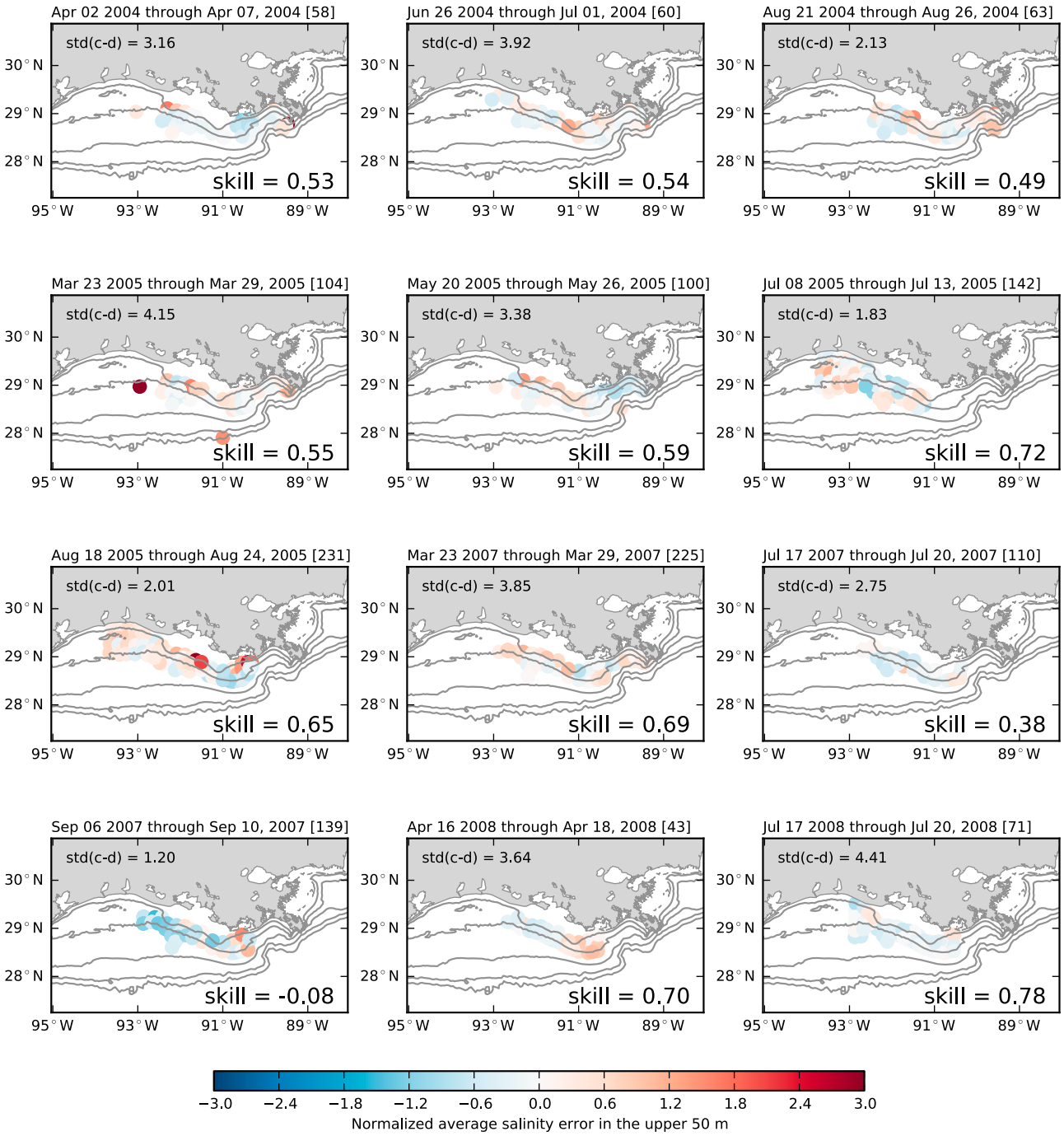

Figure 4. Errors between the model simulated salinity and the MCH measurements averaged over the upper 50 m of water column and normalized by the standard deviation of the difference between the MCH measurements and climatological values for 12 MCH data collection periods show the spatial patterns of model error for this set of hydrographic measurements. The standard deviation of the difference between the observed and climatological values and model skill are provided for each panel.

south orientation in south Texas to the east-west orientation in east Texas and Louisiana. Surface winds over the shelf are quite uniform in direction and generally blow toward the coast (southeasterlies). Although the horizontal variation of wind direction is small, the curvature of the coastline creates dramatic differences in the alongshore component of wind (this is more clearly shown in Figure 7, as will be discussed below), as suggested by *Cochrane and Kelly* [1986]. Alongshore winds are up coast over the south Texas shelf and down coast over the Louisiana shelf. Correspondingly, the wind-driven alongshore currents flow in opposing directions in the transition zone and convergence occurs as a result. When northeasterlies prevail over the shelf, alongshore currents are consistently down coast over the entire

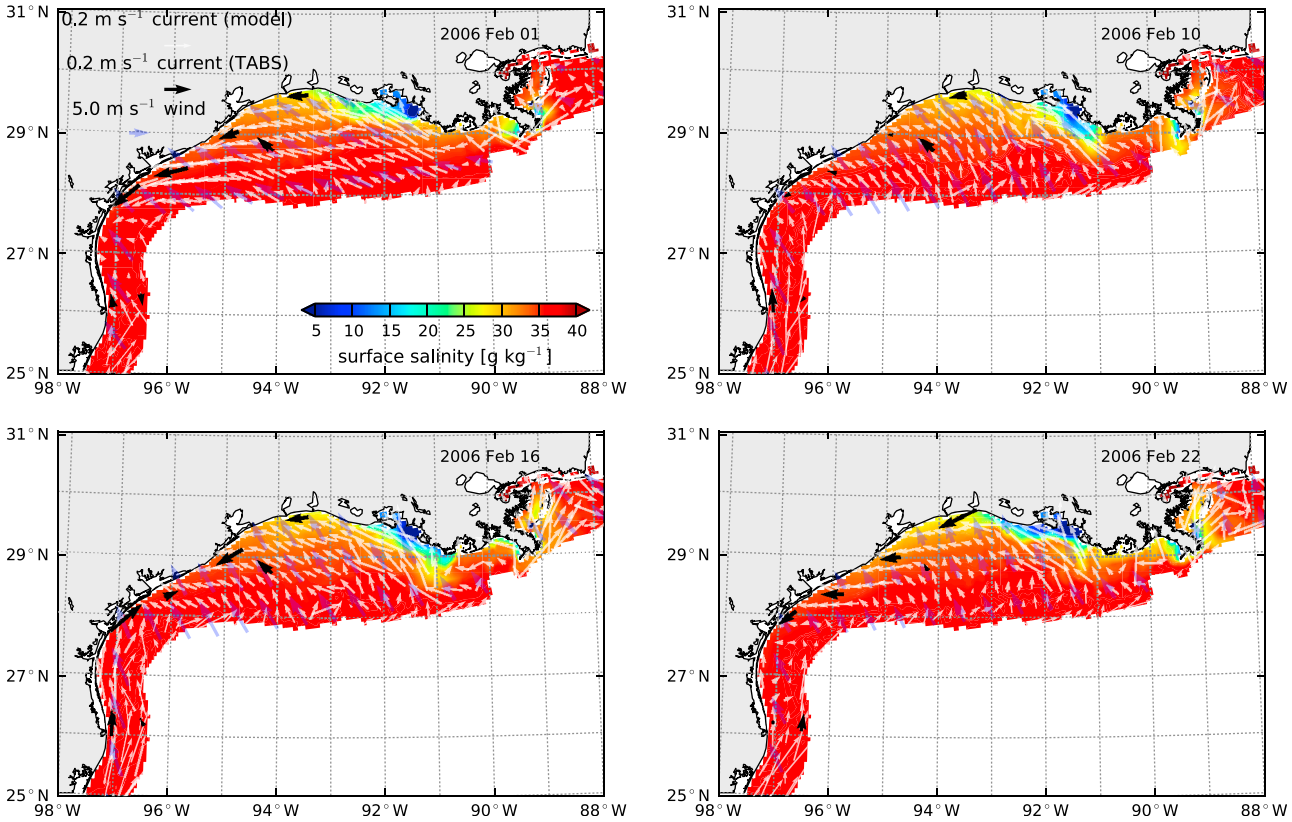

Figure 5. Snapshots of surface currents (white arrows), wind (blue arrows), and salinity fields from model and surface currents from the TABS data (black arrows) in February 2006 when convergent flows were observed. Regions deeper than 200 m are masked out because the model does not contain information about deepwater currents, in particular, the Loop Current.

shelf, and no convergence is observed. The TABS observations also show the existence of convergent flows at the snapshots in Figure 5, and the model simulated convergence locations are basically consistent with those revealed from observations for 1, 10, and 22 February. For 16 February, the simulated convergence point is located down coast of the observed convergence location.

[18] Typically, a convergence event can last for several hours up to 2–3 days, depending on the duration of the wind blowing toward the coast. In wintertime, cold frontal passages occur frequently and they usually drive intensified down-coast flows over the Texas-Louisiana shelf [*Nowlin et al.*, 2005], which destroys the convergence events. Figure 6 shows the temporal evolution of a convergence event from 16 to 19 February 2006 and how it is terminated by a frontal passage. Convergent flows are well developed at 00:00 of 16 February near the coast at about 28°N (Figure 6a). The convergence maintains its location at 12:00 of 16 February (Figure 6b) and moves slightly down coast at 00:00 of 17 February (Figure 6c). At 12:00 of 17February (Figure 6d), the coastward wind has a dramatic decrease in strength and is more aligned toward the west. With the change of wind the convergence location moves down coast to 27°N. At 00:00 of 18 February (Figure 6e), down-coast wind prevails over most of the shelf except for the southernmost section, and the convergence location moves farther down coast to 26°N. The entire shelf is dominated by down-coast wind at 12:00 of 18 February (Figure 6f) and the wind strengthens until 00:00 of 19 February (Figure 6g). Down-coast currents form over the entire extent of the shelf and the convergence disappears.

3.2. Spatial Relation Between the Convergence in Current and Wind

[19] To better show along-coast variations in the alongshore wind and current, as well as the locations of convergence, we defined a series of cross-shore transects that are placed along the coastline all the way from the south Texas coast to the central Louisiana coast near the Atchafalaya River mouth (Figure 1). These transects extend from the coastline offshore to the 30 m isobath. Wind and current values on the model grid are interpolated onto points on these transects and the alongshore components are computed for each point, and then the average value over all the points of a transect is used to represent the value of this transect. Figure 7 presents the along-coast distribution of alongshore wind and currents from four times in February 2006 corresponding to the snapshots in Figure 5. We see that, from the south Texas coast to the Louisiana coast, both the alongshore wind and surface currents change from the up-coast (positive) to down-coast (negative) direction; the zero-crossing points are the locations where convergence occurs. The convergence locations of the currents do not overlap those of the wind, but current convergence locations are shifted down

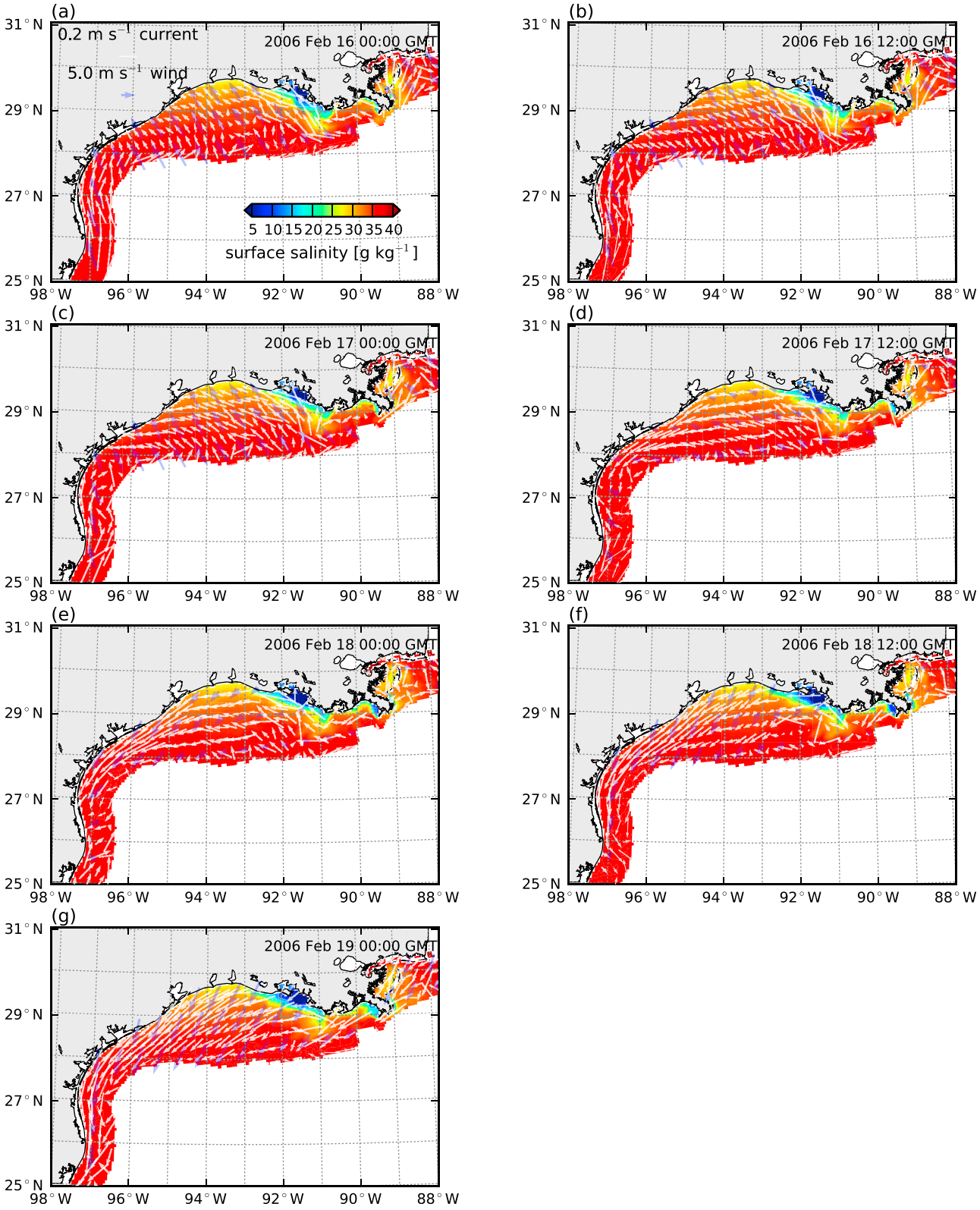

Figure 6. A time sequence of surface currents (white arrows), wind (blue arrows), and salinity fields from the model show the temporal evolution of a convergence event and how it is terminated by the passage of a cold front in wintertime. The time interval between consecutive snapshots is 12 h. Regions deeper than 200 m are masked out.

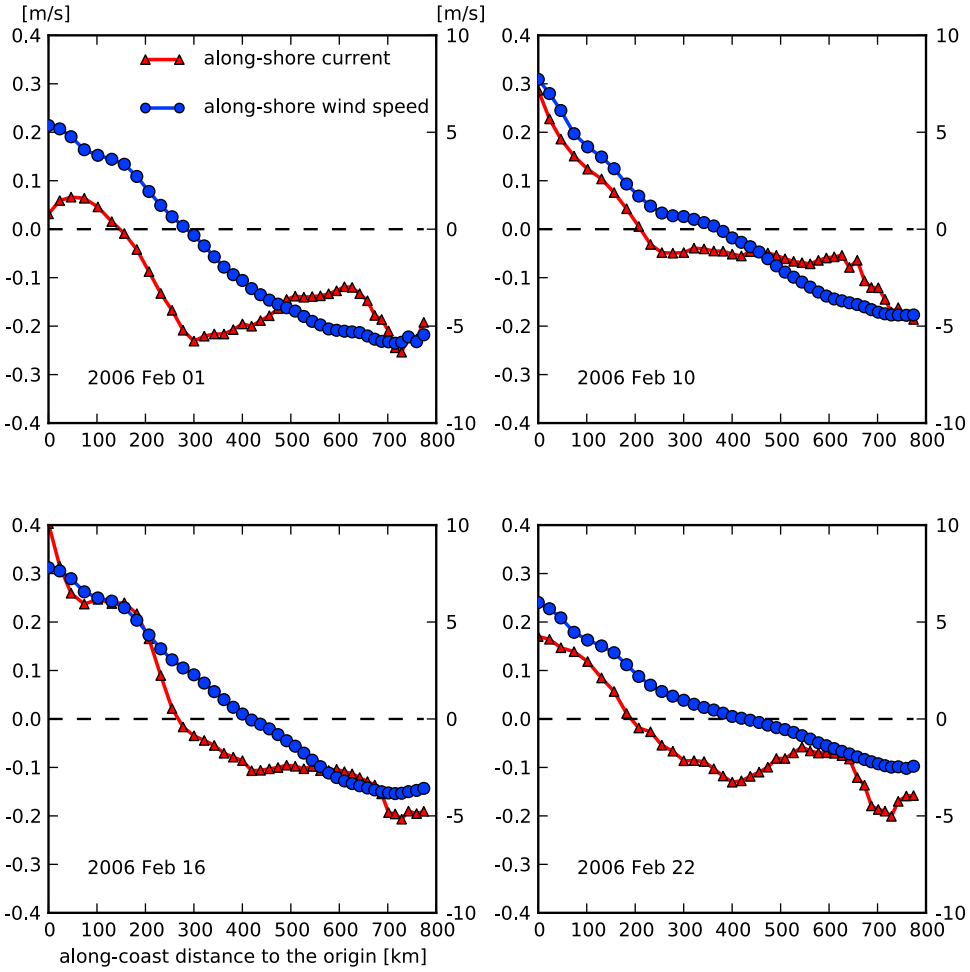

Figure 7. The along-coast distribution of alongshore wind (blue lines) and alongshore surface currents (red lines) is computed from the cross-shore transects for the same time periods as the snapshots in Figure 5. Positive values denote up-coast-directed winds or currents, and negative values indicate the down-coast direction. The zero-crossing point of each curve is the location where convergence occurs.

coast relative to the wind convergence locations. At the zero-crossing point of alongshore wind, there is still down-coast current, while at the zero-crossing point of alongshore current, the alongshore wind is up-coast. The offset between the convergence locations of currents and wind is between 100 and 200 km. The non-wind-driven flow can be roughly estimated by the value of down-coast current at the location of zero wind forcing in Figure 7, and for the four snapshots the estimates are 0.21 m s^{-1}, 0.04 m s^{-1}, 0.1 m s^{-1} and 0.12 m s^{-1}, respectively.

[20] This shift in the convergence locations of the currents indicates that there are other factors that can drive down-coast flow besides wind forcing. One likely factor is buoyancy forcing associated with the Mississippi-Atchafalaya river plume. The plume is attached to the coast and contributes to the buoyancy of the nearshore water. This sets up a positive cross-shore density gradient away from the coast, which tends to drive down-coast currents through a thermal wind balance [e.g., *Yankovsky and Chapman*, 1997]. Another factor could be continental shelf waves that propagate information from the east down coast and introduce non-locally forced currents. Wind forcing is integrated following a characteristic for a particular shelf wave mode, so a particular shelf wave mode carries the memory of previous wind conditions [*Gill and Schumann*, 1974]. This, too, would tend to shift the convergence point of currents down coast. As currents in up-coast locations are always associated with down-coast flow, shelf waves will tend to carry the memory of this down-coast, wind-forced flow farther down coast. Continental shelf waves on the Texas-Louisiana shelf have been observed by *Nowlin et al.* [1998b].

3.3. Wind Influence

[21] To further study the relation between surface alongshore currents and wind speed, scatter plots are made for the two variables for three winter months: January, February, and March of 2006 (Figure 8a). The strong correlation between currents and wind has been observed in many previous studies; for example, *Whitney and Garvine* [2005] used this relation to estimate wind influence on the Delaware coastal currents. The plots in Figure 8 reveal a positive correlation between surface current and wind speed, with $r^2 > 0.75$ for all transects except those located between the 200 km and 400 km location. This is the zone where convergence frequently occurs, and, as discussed above, the alongshore

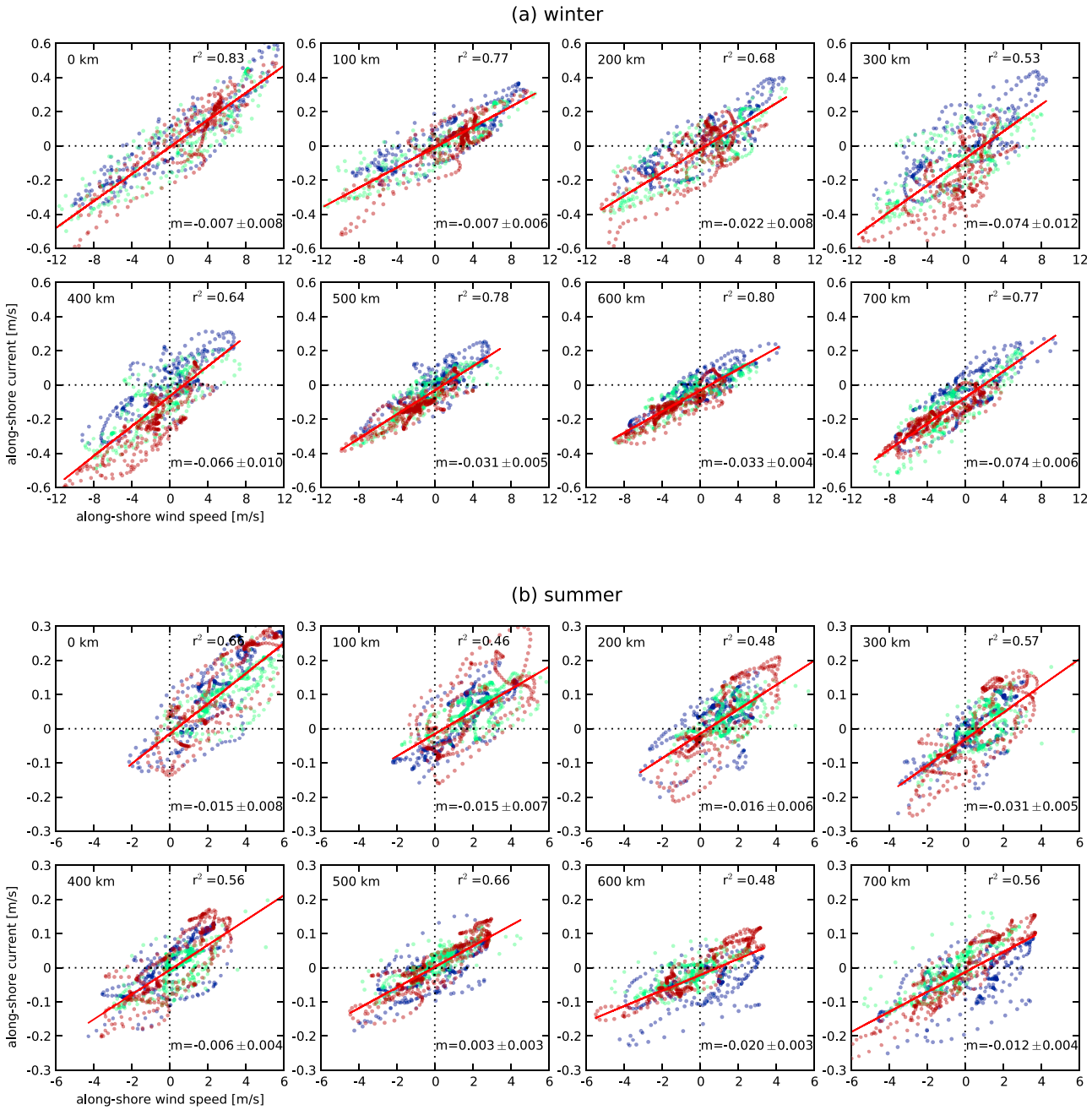

Figure 8. Scatterplots of 3-hourly surface alongshore currents versus alongshore wind speed for the 0, 100, 200, 300, 400, 500, 600, and 700 km transects shown for (a) three winter months (January (purple dots), February (green dots), and March (maroon dots)) and (b) three summer months (June (purple dots), July (green dots), and August (maroon dots)) of 2006. Linear regression is performed for each plot, and the corresponding r^2 value is provided. Also provided is the y intercept value (m) of the regression line at the 95% confidence level.

current is not quite in phase with the local alongshore wind at convergence locations, thereby reducing the correlation somewhat. There is clearly a hysteresis in the lagged response of currents to the wind that causes the cloud of points to spread to an oval shape, instead of an exact linear relationship. However, there is also clearly a shift in the correlation toward the fourth quadrant, with down-coast currents under up-coast winds occurring more often than the opposite case. This suggests that there is a mean down-coast flow during times of convergence similar to that expected for buoyancy forcing or continental shelf waves. The magnitude of this flow can be estimated by the y axis intercept, which denotes current under zero wind forcing. For all the transects the y axis intercept values are negative, meaning that there are down-coast currents when wind forcing disappears. The non-wind-driven down-coast current is strongest

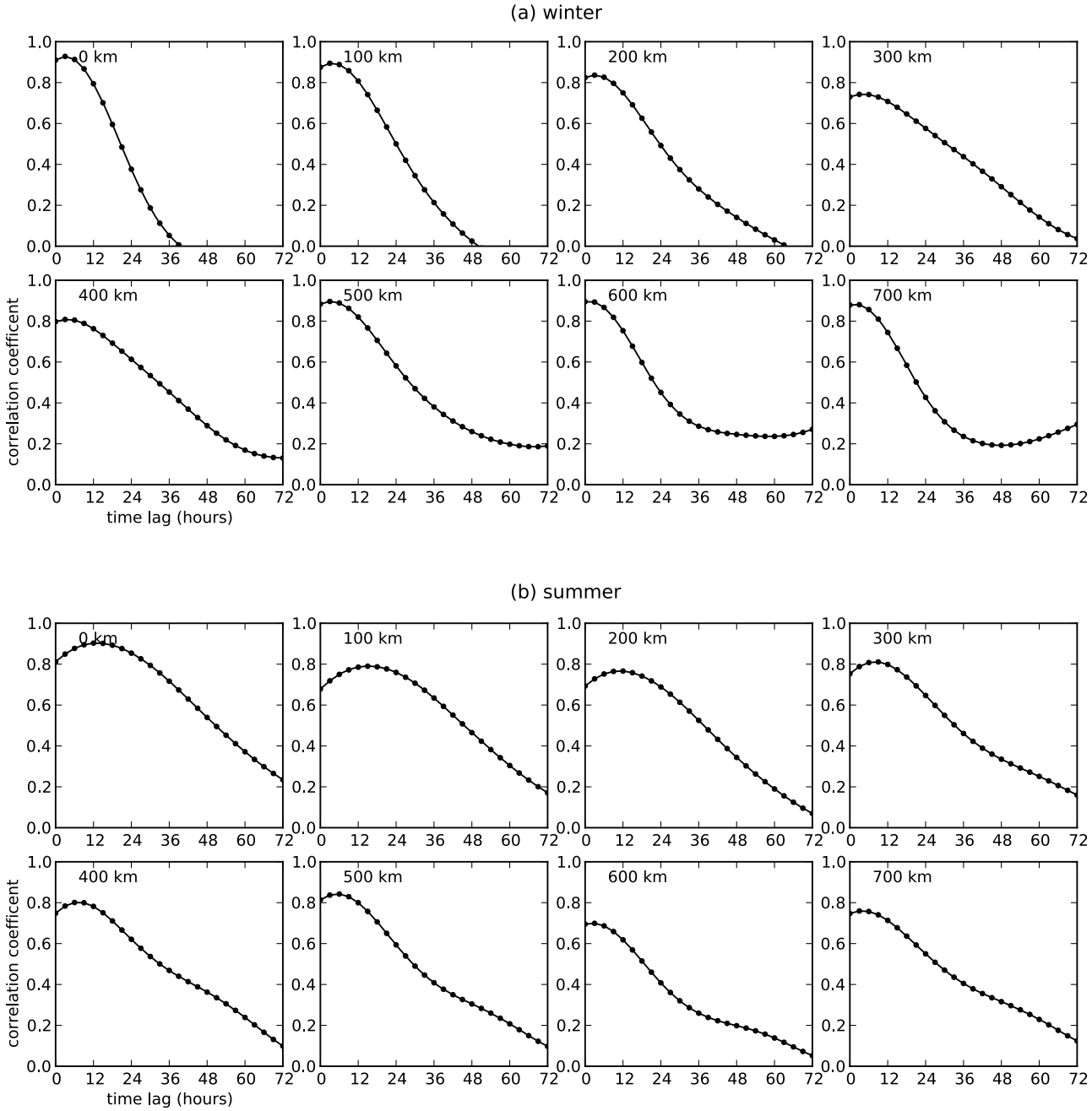

Figure 9. Time lag correlations between 3-hourly surface alongshore currents and alongshore wind for cross-shore transects in Figure 8 show that currents lag wind forcing by 3 to 12 h.

at the 300 km and 400 km transects and approximately 0.07 m s^{-1}, slightly lower but roughly the same magnitude as the four examples shown in Figure 5.

[22] Figure 9 displays the time lag correlation between the alongshore currents and wind speed for the transects shown in Figure 8. In wintertime, the two variables have very high correlation (over 0.8 for most of the transects) at time lag 0, and the highest correlation occurs when surface currents lag behind wind for 3 h. After 3 h, the correlation coefficient shows exponential decay within the time lag of 48 h except for the 300 and 400 km transects, and the e-folding time scale is between 20 and 60 h. For the 300 and 400 km transects, the correlation coefficient also decays with time but with a linear pattern. Therefore compared to other transects, currents at these two transects have stronger inertia. In general, the analysis between alongshore wind and surface alongshore currents in winter reveals a fast response of currents to wind on the weather band.

[23] In summer months, winds are weak and currents become sluggish (Figure 8b; note that both the range of x axis and y axis are just half of that in winter), and the correlation between surface currents and wind shows a slight reduction. Instead of near-instantaneous response to the wind forcing as in winter, the currents display more inertia,

in that the highest correlation between currents and wind occurs at a longer time lag, e.g., ~12 h for transects south of the 300 km location. Also, there is a weaker decay of the correlation with increasing time lag. The long time lag may be a consequence of relatively weak wind forcing. However, we do observe prominent convergent flows in summertime under strong wind conditions, and their characteristics are similar to those in winter. As mentioned above, the more disorganized currents in summer generally render the convergence pattern more complex than in winter, and the long correlation time lag may play an important role in this.

3.4. Buoyancy Influence

[24] In coastal regions with inflow of fresh water, buoyancy can play a significant role in driving alongshore currents through an offshore density gradient created by the fresh water plume. The buoyancy-induced alongshore current can be estimated by the thermal wind balance:

$$u_z = \frac{g}{f\rho_0}\rho_y, \tag{2}$$

where u is the alongshore velocity, g is the gravitational acceleration, f is the Coriolis parameter and ρ_0 is the reference density; the subscript z and y denote vertical and cross-shore gradient, respectively. Figure 10 presents the vertical profiles of mean salinity, temperature and density of a cross-shore transect near 28°N (about the 300 km location) over January, February, and March of 2006. The isohalines (Figure 10a) are more vertically aligned due to strong vertical mixing in the winter season, and salinity increases in the offshore direction as a result of fresh water from the Mississippi and Atchafalaya rivers introduced at the coast. The horizontal gradient of salinity is slightly larger inshore of the 40 m isobath than offshore. The plume on the whole displays a pattern that is similar to the "bottom-advected plume" described by *Chapman and Lentz* [1994] and *Yankovsky and Chapman* [1997]. Temperature (Figure 10b) also increases offshore, attributed to the distribution of solar radiation, greater cooling of the shallow coastal water under wintertime surface heat loss and the presence of cold plume water along the coast. Salinity is the major determinant of density, and the isopycnals (Figure 10c) also have a stronger gradient inshore of the 40 m isobath; the highest horizontal gradient occurs in the area between the 25 and 35 m isobath. Using this density profile, we estimated the alongshore velocity at each depth level by vertically integrating equation 2 and assuming a zero bottom velocity, as in *Yankovsky and Chapman* [1997]. The resulting profile of alongshore current is shown in Figure 10d. This analysis suggests that buoyancy can induce down-coast currents of approximately 0.12 m s^{-1} near the surface. In the high-density gradient region between the 25 and 35 m isobath, the largest alongshore surface current is ~0.14 m s^{-1}. Averaging the surface alongshore velocity over the span from the coastline to the 30 m isobath yields a value of 0.12 m s^{-1}. This number is slightly larger than the estimated buoyancy-driven current for the 300 km transect (~0.07 m s^{-1}) in Figure 8, but it is close to the average value of the estimated non-wind-driven down-coast currents from the four examples in Figure 5. This could be an indication that buoyancy forcing contributes to most of the non-wind-driven currents and thus the offset between convergent currents and winds. The profile for model-produced mean alongshore flow over January, February, and March of 2006 is presented in Figure 10e. The mean flow field shows overall a baroclinic structure that is similar to the buoyancy-driven flow field (Figure 10d). This suggests that the thermal wind balance is a good approximation of the shelf dynamics on seasonal scales. The buoyancy-driven alongshore flow overestimates the mean alongshore flow at surface and underestimates the mean flow at bottom. Bottom velocity of the mean flow field is not zero as in our assumption, indicating that the bottom flow has a barotropic component that is introduced by wind.

[25] We also conducted a control model run in which the Mississippi-Atchafalaya river forcing is taken out, as a way to test the effect of buoyancy on the convergence. The locations of convergent surface currents and winds for the same snapshots in Figure 5 are shown in Figure 11, but for the case with no river discharge. Without buoyancy forcing, convergence still occurs at these times, confirming that wind is the determining factor for the formation of convergent flows. However, there is a marked shift in the location of convergent currents compared to that in Figure 7, such that the convergent flows now occur very close to the locations of convergent winds. This, again, suggests that buoyancy forcing is the primary factor leading to the offset between the convergent currents and winds. For 10 February, the down-coast drift of convergent currents from winds are still observed, implying that besides buoyancy forcing, continental shelf waves may also play a role in forcing down-coast currents.

3.5. Temporal Variation of Convergent Flows

3.5.1. Weather Band Pattern

[26] As the winds are highly variable over time scales of roughly 3–10 days, the weather band, it is expected that convergence of wind and currents also have strong temporal variations. Figure 12 displays the along-coast distribution of 3-hourly alongshore wind (Figure 12, left) and surface currents (Figure 12, right) varying with time in 2006 winter and spring. No band-pass filtering is applied to the 3-hourly data. A fourth-order polynomial function is fit to the spatial distribution curve for each time moment to find out the convergence location where alongshore values change from up-coast (positive, red color) to down-coast (negative, blue color). We see that the 3-hourly wind displays a strong variability over time, and correspondingly the convergence of wind occurs over a broad range of spatial scales (the black dots are spread over 0–800 km). The alongshore currents make a similar pattern to that of the alongshore wind. Because the time series is not filtered, near-inertial motions are clearly seen as the stripped patterns with a cycle of ~1 day. The near-inertial motions are particularly strong between 15 March and 15 May. This is because the wind field is gradually dominated by diurnal signals from spring to summer, and as the vertical stratification strengthens, frontal passages are less common, and more inertial band energy is trapped in the surface layer [*Zhang et al.*, 2009, 2010]. The convergence point of the currents is also spread over a wide range, but its variability is not as high as that of wind. Most of the convergent currents occur between the 100 and 500 km location, and these locations are generally down coast of the

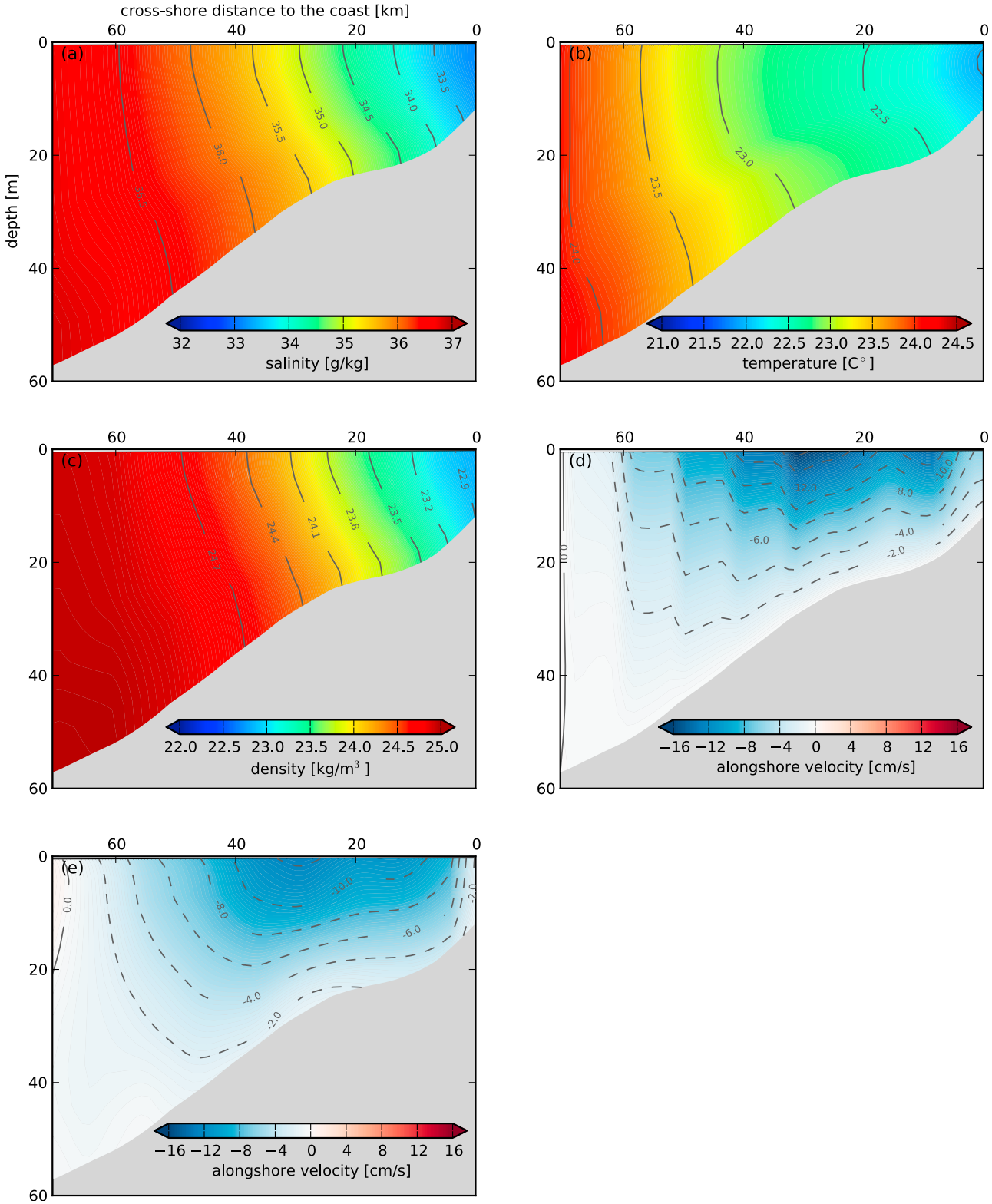

Figure 10. Vertical profiles of mean (a) salinity, (b) temperature, (c) relative density, (d) alongshore velocity derived from thermal wind balance, and (e) alongshore velocity from model results over January, February, and March of 2006 for a cross-shore transect near 28°N.

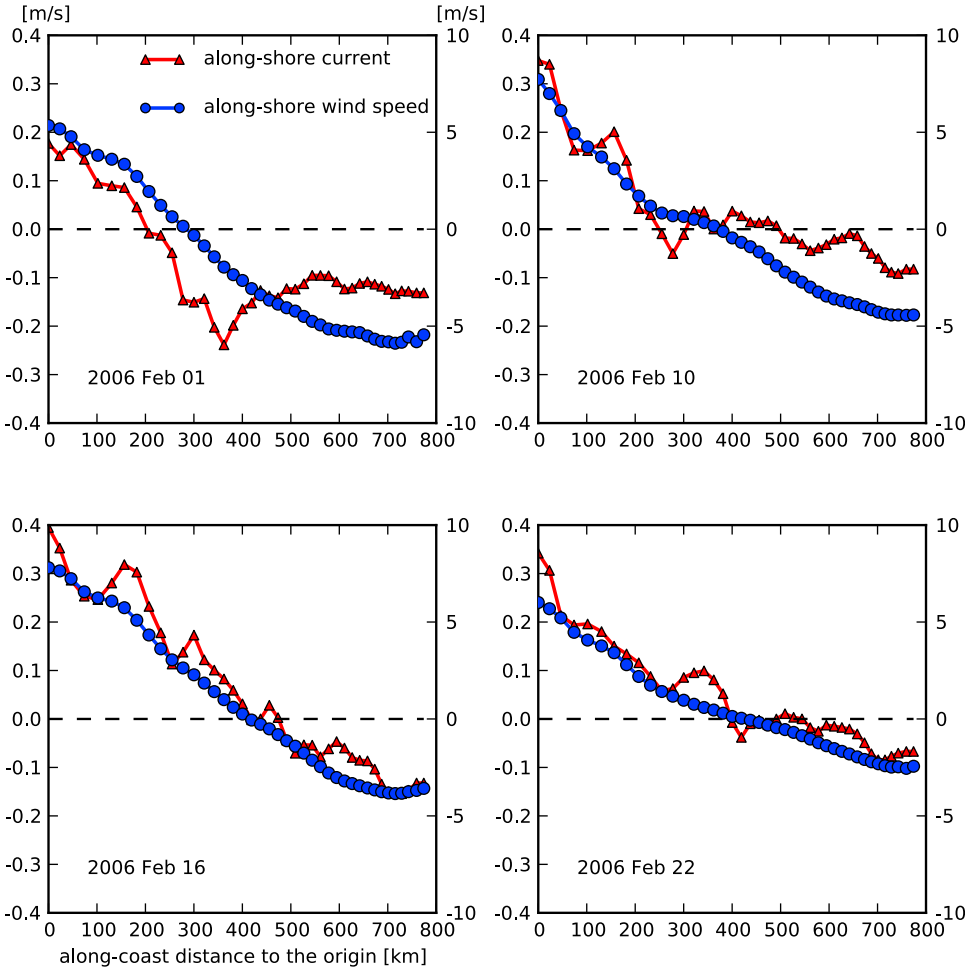

Figure 11. Same as Figure 7, but for the control run in which river forcing is taken out.

wind convergence points. For the weather band convergence, we do not find any specific trend in its temporal variation.

3.5.2. Monthly Mean Pattern

[27] Seasonal-scale convergence has been mentioned in several studies, but very few have analyzed its temporal variation. Only *Morey et al.* [2005] suggested that there is a seasonal migration of monthly convergence location along the coast. Here we will provide a more thorough discussion on seasonal variation of the monthly convergence pattern. Compared with *Morey et al.* [2005] that uses monthly climatology wind forcing in its model, our study uses the real-time wind forcing, allowing us to investigate the interannual variability of monthly convergence. Figure 13 (left) shows the along-coast distribution of monthly mean alongshore wind and surface currents varying with month in 2006. The monthly mean convergence displays a prominent seasonal pattern. The convergence of wind generally migrates up coast in spring and summer, with an exception due to anomalous winds in January with anomalous weak down-coast winds over the northern section of the coast opposed by anomalous strong up-coast winds from south, shifting the convergence point farther up coast relative to the locations in normal winter months. As down-coast winds strengthen in February, the convergence point of the wind retreats back to the 100 km location, and with the development of up-coast winds and their intrusion toward the upper coast in spring and summer, convergence marches up coast all the way to the 500 km location in July. Thereafter, down-coast winds begin to gain strength and their down-coast intrusion forces the convergence location to retreat all the way down coast until November. In December, the study area is dominated by down-coast winds and no convergence is observed. The evolution of convergent currents bears close resemblance to the wind pattern, but in October convergent flows are not obviously seen, and they might have moved farther down coast to the east Mexico shelf, an area that is included in the studies of *Morey et al.* [2005] and *Zavala-Hidalgo et al.* [2003]. A comparison between the locations of convergent currents and winds shows that for most months (February, March, April, June, July, September, and November), the convergent currents occur down coast of the convergent winds, but the offset is generally less than 100 km, smaller than the snapshot values. A possible reason is that, on seasonal scales, the effects of weather band dynamical features (like shelf waves) on currents decrease, resulting in more consistent flow and wind patterns.

[28] The seasonal pattern of monthly mean convergence has interannual variability. Figure 13 (middle) also presents the convergent winds and currents in 2009, which is notable for its anomalously strong up-coast winds. We see that in

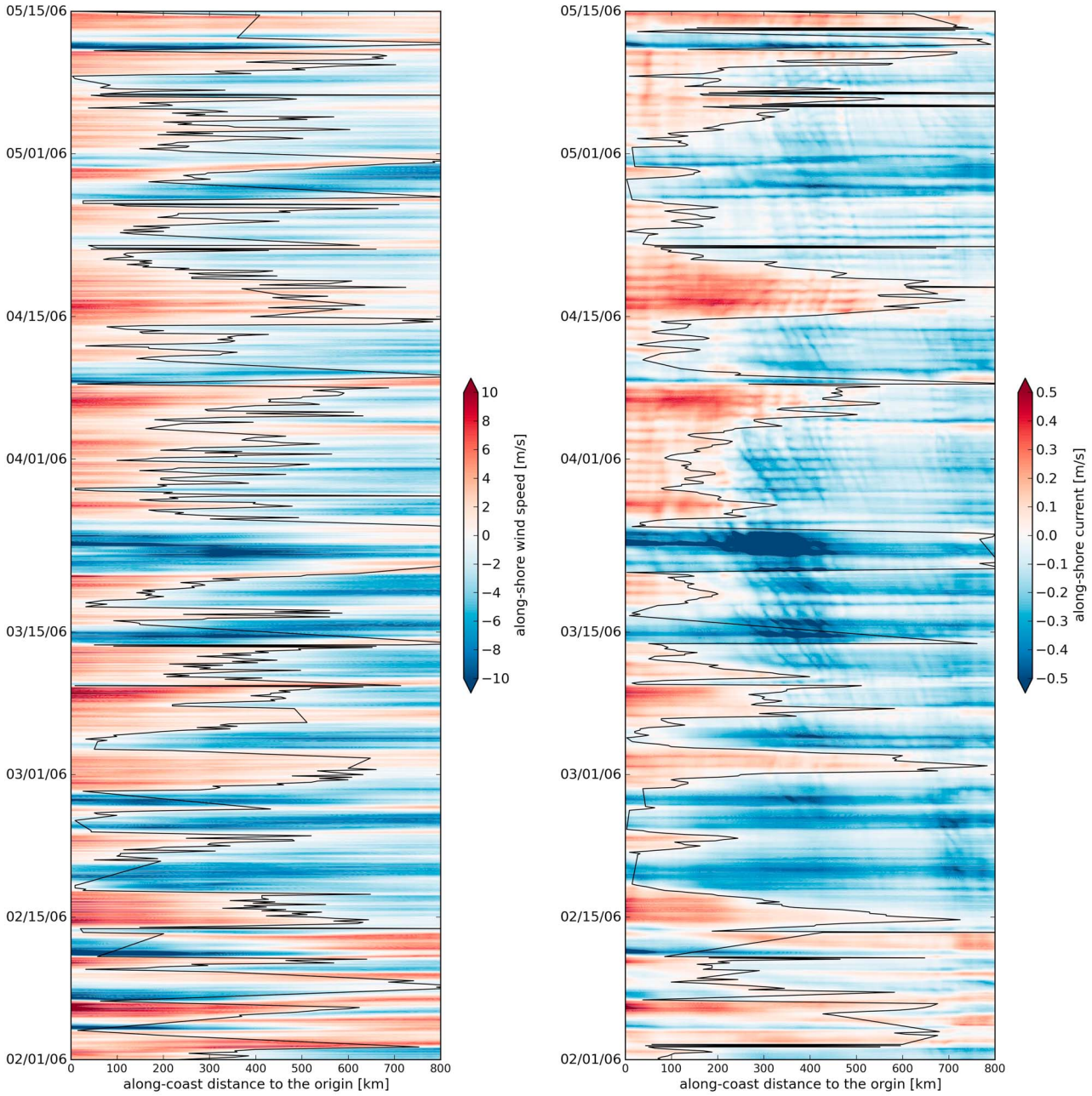

Figure 12. The Hovmöller diagram of nonfiltered 3-hourly (left) alongshore wind speed and (right) alongshore surface currents from the model for 2006 winter and spring shows the evolution of alongshore wind and currents in time. The x axis is the along-coast distance to the origin, and the y axis is date. Up-coast values are positive and are represented by red colors, while down-coast values are negative and are represented by blue colors. The black dots mark the locations of convergence. The convergence location for each time moment is found out by fitting a fourth-order polynomial function to the spatial distribution curve for wind and currents at this moment and then locating the zero-crossing point of the polynomial function.

summer months, up-coast winds have greater strength than those in 2006, and they also reach much farther up coast so that convergence of wind does not occur in the study region. The marching of convergence of currents basically follows that of wind in spring (February to May) and fall (September and October), and in June and July no convergent currents are observed.

[29] Seasonal variation of convergence based on a 10 year (2001–2010) average is shown in Figure 13 (right). The average decadal pattern shows that convergence initially

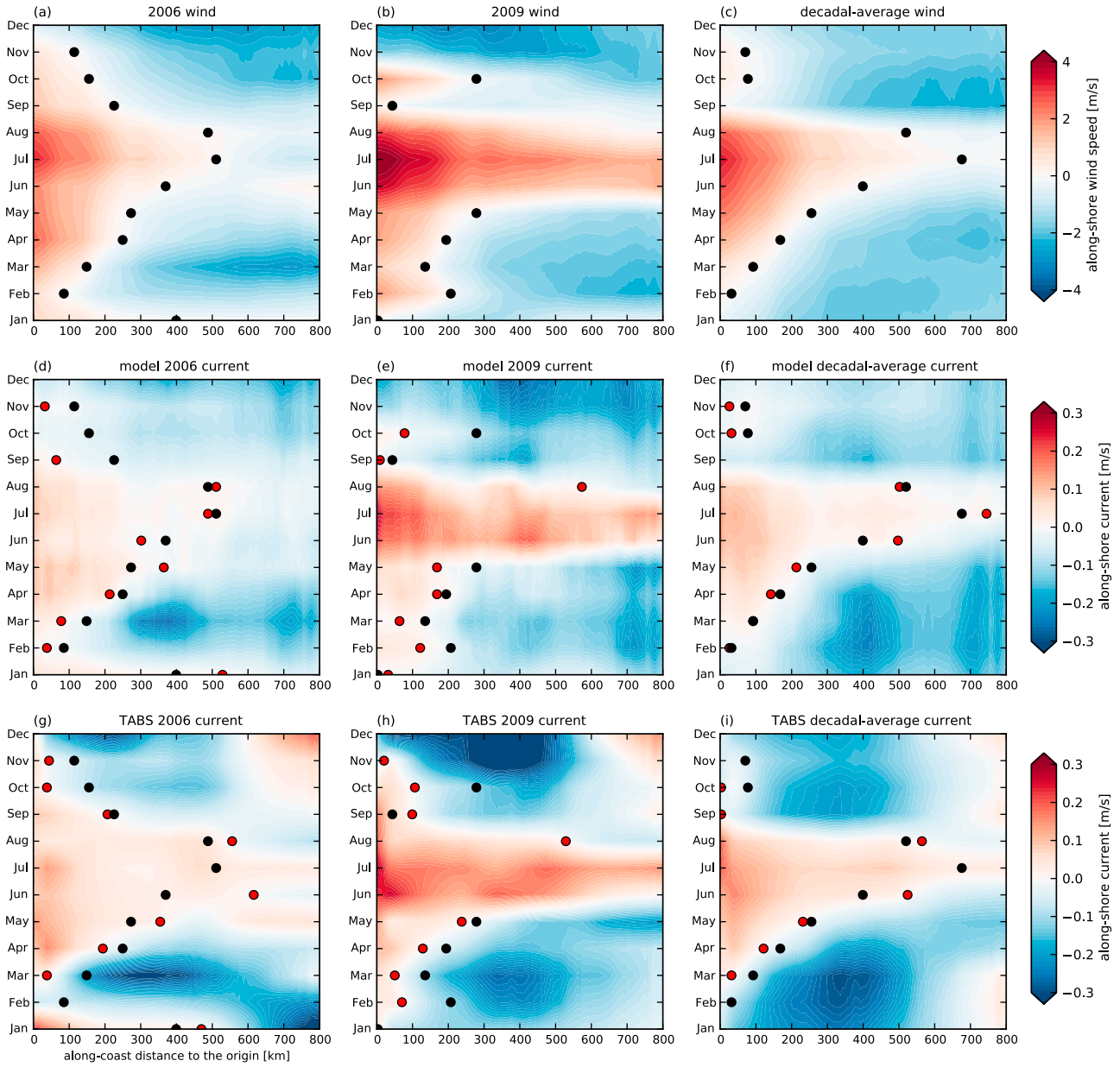

Figure 13. The Hovmöller diagrams of monthly mean (a–c) alongshore wind speed, (d–f) alongshore surface currents from the model, and (g–i) alongshore surface currents from the TABS buoys for the year (left) 2006, (middle) 2009, and (right) 10 year average show that there is significant seasonal and interannual variability in the convergence locations of currents and wind. The x axis is the along-coast distance to the origin, and the y axis is month. Up-coast values are positive and are represented by red colors, while down-coast values are negative and are represented by blue colors. The black dots mark the locations of convergent winds, and the red dots mark the locations of convergent currents.

develops in February within the study region. The up-coast migration of convergence from spring to summer and down-coast retreat in fall and winter is similar to the 2006 case, while in summer months the convergence location reaches farther up coast relative to 2006, as a result of greater intrusion of up-coast winds. But this intrusion is not as strong as in 2009, and convergence of wind and currents can still be observed in the study area.

[30] We also investigated the monthly mean pattern of convergence using the TABS data (Figures 13g–13i). These data are sparsely distributed in space and cannot resolve the convergence locations exactly, but we do anticipate that a seasonal pattern may be revealed by these observations. We only use the data from the inner-shelf buoys, since dynamics of the outer shelf are different from that of the inner shelf, and including the offshore buoy data can bias the results. Surface velocity data from bouys B, D, F, J, K, R and W are interpolated onto the cross-shore transects and rotated to the alongshore direction. Results of the monthly mean convergence are shown in Figures 13g–13i. As we expected, in

spite of their low spatial resolution, the TABS data still reflect a seasonal variation for convergence very similar to that calculated from the numerical simulation.

4. Discussion

[31] The local response of alongshore currents to alongshore wind can be investigated by a barotropic friction model. The slope burger number, defined as $\alpha^2 N^2/f^2$ [*Clarke and Brink*, 1985], is $\ll 1$ for most of the Texas-Louisiana shelf in the winter seasons (based on our computations and hydrographic observations), where α is the average shelf bottom slope and N^2 the buoyancy frequency. This suggests that a barotropic model is appropriate for describing the shelf dynamics here [*Clarke and Brink*, 1985; *Lentz*, 2008], while *Jarosz and Murray* [2005] also demonstrated that in wintertime there is a predominant barotropic response of the inner shelf currents to strong winds. The depth-averaged alongshore momentum equation is written as

$$\frac{\partial u}{\partial t} - fv = -g\frac{\partial \eta}{\partial x} + \frac{F^x}{H} - \frac{ru}{H}, \tag{3}$$

where u is the depth-averaged alongshore velocity, v is the depth-averaged cross-shore velocity, η is the surface elevation, F is the kinematic alongshore wind stress, r is a linear bottom drag coefficient and H is the water depth. The bottom friction term acts as an energy sink, and equating the scales of this term and the local acceleration term gives a frictional spin-down time scale of $T \sim H/r$. If we take the linear bottom drag coefficient r as 3×10^{-4} m s^{-1} for the Texas-Louisiana shelf following *Jarosz and Murray* [2005], and an average depth of 15 m inshore of the 30 m isobath, we obtain a decay time of 14 h. The magnitude of this value is roughly the same as that of the decay scale derived from the autocorrelation analysis in section 3.3. Discrepancies could arise from baroclinic factors that are not represented in this barotropic friction model.

[32] The model results suggest that the offset between the wind and current convergence points cannot always be explained entirely by buoyancy forcing, although buoyancy forcing does appear to be the dominant factor in creating this offset. Continental shelf waves are most likely responsible for the remaining balance, and for long time scales in shallow water where bottom friction may be an important factor, the residual flow caused by shelf waves may be explained by arrested topographic wave theory [*Csanady*, 1978]. The distance between a local current regime and the farthest wind source influencing it can be estimated by the alongshore decay scale of the topographic waves. A scaling analysis of the governing equation for the arrested topographic wave, derived by *Csanady* [1978], suggests the decay scale is $X \sim fHY/r$, where X, Y and H denote the alongshore, cross-shore and vertical scales, respectively. Taking the same values for r and H as used above, and assuming a cross-shore scale Y of 50 km with an average Coriolis parameter of 7×10^{-5} s^{-1} for the shelf, we obtain an alongshore decay scale of $X \sim$ 170 km. This scale is the same order as the spatial offset of the wind and current convergence points, and so we conclude that shelf waves could possibly have an influence in shifting the convergence point of currents down coast.

[33] Eliminating the river forcing could also have a nonlinear influence on other dynamical aspects, such as the response of currents to local winds and shelf waves, or changes in bottom drag. The offshore density gradient tends to establish a thermal-wind-balanced vertical shear that reduces the alongshore velocity near the bottom, thus reducing bottom drag relative to what would be estimated only considering the vertical mean flow. So, once this density gradient is eliminated, the bottom drag may be enhanced, which in turn leads to a decrease in the spin-down time scale, and a faster response of currents to local winds. Also, as bottom drag increases, the alongshore decay scale of shelf waves decreases, and a reduction in the nonlocal effect of winds might be expected.

[34] Convergence of alongshore currents can be compensated by offshore transport. Such transport has been reported by previous studies on the freshwater transport over the western shelf of the Gulf of Mexico. *Zavala-Hidalgo et al.* [2003] suggested that an offshore transport of at least 0.1 Sv can be generated by the convergence in the Bay of Campeche. *Morey et al.* [2005] found the most vigorous cross-shore export of freshwater occurring during spring and fall in the convergence region of the Texas-Louisiana shelf. A recent study of the Mississippi and Atchafalaya freshwater transport over the Texas-Louisiana shelf [*Zhang et al.*, 2012b] observed a up-coast migration of freshwater outflow from winter to summer, and it is inferred that this is associated with the seasonal migration of the convergent currents.

5. Conclusions

[35] This study investigates convergent surface alongshore flows on the inner Texas-Louisiana shelf with a numerical model. Comparisons with observations show that the model has a reasonable ability to reproduce observed shelf-scale surface current, salinity, and surface elevation fields.

[36] Convergent flows are studied on both the weather band and seasonal time scales. The model predicted convergence locations are supported by moored current observations. This study finds a close relation between the formation of convergent flows and spatial variation in the alongshore component of wind forcing. Convergent flows are typically associated with broad-scale landward blowing winds. While the wind direction is nearly uniform over the entire shelf, the alongshore component of wind changes with the curving coastline. The curving coastline causes the alongshore wind to undergo a reversal from the south Texas coast to the Louisiana coast. The reversal in the alongshore wind direction causes a reversal in the alongshore current direction, resulting in a convergence zone. For the weather band, convergence events can last from several hours to several days, and in winter seasons they are usually ended by the passage of cold fronts that drive intensified down-coast currents along the entire shelf.

[37] In wintertime, surface alongshore currents have a swift response to alongshore wind variations for most of the inner shelf region, and the two variables follow a quite linear relationship with high correlation, confirming that alongshore wind is the dominant factor in the formation of convergent alongshore flows. In summertime, both winds and currents are weak and currents are less sensitive to wind changes, and under the more disorganized flow patterns

convergent events are hard to distinguish. We attribute this in part to the longer response time of the currents to the wind.

[38] Examination of the locations of convergent currents and winds reveal that the convergence locations are not colocated, but rather converging currents usually occur down coast of converging winds. Two factors could contribute to the down-coast shift of the convergent currents: buoyancy forcing that can drive down-coast currents through the offshore density gradient due to the Mississippi-Atchafalaya river plume, and continental shelf waves that propagate down coast and generate nonlocally forced currents. Results from a control model run which excludes river forcing show that buoyancy forcing is most likely the primary factor for causing the offset between the converging currents and winds, while continental shelf waves may also play a role. Also, the magnitude of buoyancy-driven, alongshore currents estimated from the thermal wind balance indicates that this buoyancy-driven flow is similar in magnitude to the observed down-coast flow under no wind forcing.

[39] As the weather band winds are highly variable over time, the convergent alongshore wind locations can occur over a broad stretch of the Texas and Louisiana coastlines. The weather band converging currents also show a temporal variability, but their occurrence is basically confined between Galveston Bay and Baffin Bay of Texas. No specific temporal pattern is found for the weather band convergence. However, the monthly mean convergent winds and currents clearly reveal a seasonal pattern based on both model and observational results. While having marked interannual variability, convergence typically appears in the southern section of the Texas-Louisiana shelf in early spring and marches up coast with the transition of prevailing winds over the shelf from down-coast in winter to up coast in summer. This up-coast migration stops in midsummer, and as down-coast winds begin to dominate again, the convergence location retreats southward until late winter.

[40] **Acknowledgments.** This study is funded by the Texas General Land Office through TGLO TABS Modeling Effort (award 08-054-000-1146) and TGLO Improving Hydrodynamic Predictions (award 10-096-000-3927). We thank Steve DiMarco at Texas A&M University for providing the Mechanisms Controlling Hypoxia data. The data from TCOON and SEAMAP are also appreciated.

References

Chapman, D. (1985), Numerical treatment of cross-shelf open boundaries in a barotropic coastal ocean model, *J. Phys. Oceanogr.*, *15*, 1060–1075.

Chapman, D., and S. Lentz (1994), Trapping of a coastal density front by the bottom boundary layer, *J. Phys. Oceanogr.*, *24*(7), 1464–1479.

Cho, K., R. O. Reid, and W. D. Nowlin Jr. (1998), Objectively mapped stream function fields on the Texas-Louisiana shelf based on 32 months of moored current meter data, *J. Geophys. Res.*, *103*(C5), 10,377–10,390, doi:10.1029/98JC00099.

Clarke, A., and K. Brink (1985), The response of stratified, frictional flow of shelf and slope waters to fluctuating large-scale, low-frequency wind forcing, *J. Phys. Oceanogr.*, *15*(4), 439–453.

Cochrane, J. D., and F. J. Kelly (1986), Low-frequency circulation on the Texas-Louisiana continental shelf, *J. Geophys. Res.*, *91*(C9), 10,645–10,659, doi:10.1029/JC091iC09p10645.

Csanady, G. T. (1978), The arrested topographic wave, *J. Phys. Oceanogr.*, *8*, 47–62.

DiMarco, S. F., P. Chapman, N. Walker, and R. D. Hetland (2010), Does local topography control hypoxia on the eastern Texas-Louisiana shelf?, *J. Mar. Syst.*, *80*(1–2), 25–35, doi:10.1016/j.jmarsys.2009.08.005.

Flather, R. (1976), A tidal model of the northwest European continental shelf, *Mem. Soc. R. Sci. Liege*, *6*, 141–164.

Gill, A. E., and E. H. Schumann (1974), The generation of long shelf waves by the wind, *J. Phys. Oceanogr.*, *4*(1), 83–90.

Hetland, R. D. (2006), Event-driven model skill assessment, *Ocean Modell.*, *11*(1–2), 214–223, doi:10.1016/j.ocemod.2004.12.001.

Hetland, R. D., and L. Campbell (2007), Convergent blooms of *Karenia brevis* along the Texas coast, *Geophys. Res. Lett.*, *34*, L19604, doi:10.1029/2007GL030474.

Hetland, R. D., and S. F. DiMarco (2011), Skill assessment of a hydrodynamic model of circulation over the Texas-Louisiana continental shelf, *Ocean Modell.*, *43–44*, 64–76, doi:10.1016/j.ocemod.2011.11.009.

Hunter, R. E., L. E. Garrison, and G. E. Hill (1974), Maps showing the drift patterns along the south Texas coast, *U.S. Geol. Surv. Misc. Field Stud. Map*, *MF-623*.

Jarosz, E., and S. P. Murray (2005), Velocity and transport characteristics of the Louisiana-Texas coastal current, in *Circulation in the Gulf of Mexico: Observations and Models*, *Geophys. Monogr. Ser.*, vol. 161, edited by W. Sturges and A. Lugo-Fernandez, pp. 143–156, AGU, Washington, D. C., doi:10.1029/GM161.

Leipper, D. F. (1954), Physical oceanography of the Gulf of Mexico: Gulf of Mexico, its origins, waters and marine life, *Fish. Bull.*, *55*, 119–137.

Lentz, S. (2008), Observations and a model of the mean circulation over the Middle Atlantic Bight continental shelf, *J. Phys. Oceanogr.*, *38*, 1203–1221.

Li, Y., W. Nowlin Jr., and R. Reid (1996), Spatial-scale analysis of hydrographic data over the Texas-Louisiana continental shelf, *J. Geophys. Res.*, *101*(C9), 20,595–20,605, doi:10.1029/96JC02163.

Morey, S. L., J. Zavala-Hidalgo, and J. O'Brien (2005), The seasonal variability of continental shelf circulation in the northern and western Gulf of Mexico from a high-resolution numerical model, in *Circulation in the Gulf of Mexico: Observations and Models*, *Geophys. Monogr. Ser.*, vol. 161, edited by W. Sturges and A. Lugo-Fernandez, pp. 203–218, AGU, Washington, D. C., doi:10.1029/GM161.

Nowlin, W. D., Jr., A. E. Jochens, R. O. Reid, and S. F. DiMarco (1998a), Texas-Louisiana shelf circulation and transport processes study: Synthesis report, vol. I, Technical report, *Tech. Rep. OCS Study MMS 98-0035*, Gulf of Mexico OCS Region, Miner. Manage. Serv., U.S. Dep. of the Inter., New Orleans, La.

Nowlin, W. D., Jr., A. E. Jochens, R. O. Reid, and S. F. DiMarco (1998b), Texas-Louisiana shelf circulation and transport processes study: Synthesis report, vol. II, Appendices, *Tech. Rep. OCS Study MMS 98-0035*, Miner. Manage. Serv., U.S. Dep. of the Inter., New Orleans, La.

Nowlin, W. D., Jr., A. E. Jochens, S. F. DiMarco, R. O. Reid, and M. K. Howard (2005), Low-frequency circulation over the Texas-Louisiana continental shelf, in *Circulation in the Gulf of Mexico: Observations and Models*, *Geophys. Monogr. Ser.*, vol. 161, edited by W. Sturges and A. Lugo-Fernandez, pp. 219–240, AGU, Washington, D. C., doi:10.1029/GM161.

Oey, L. Y. (1995), Eddy-and wind-forced shelf circulation, *J. Geophys. Res.*, *100*(C5), 8621–8637, doi:10.1029/95JC00785.

Shchepetkin, A. F., and J. C. McWilliams (2005), The regional oceanic modeling system (ROMS): A split-explicit, free-surface, topography-following-coordinate oceanic model, *Ocean Modell.*, *9*(4), 347–404, doi:10.1016/j.ocemod.2004.08.002.

Watson, R., and E. W. Brehens (1970), Nearshore surface currents, southeastern Texas Gulf coast, *Contrib. Mar. Sci.*, *15*, 133–143.

Whitney, M. M., and R. W. Garvine (2005), Wind influence on a coastal buoyant outflow, *J. Geophys. Res.*, *110*, C03014, doi:10.1029/2003JC002261.

Yankovsky, A. E., and D. C. Chapman (1997), A simple theory for the fate of buoyant coastal discharges, *J. Phys. Oceanogr.*, *27*, 1386–1401.

Yuan, D., F. Qiao, and J. Su (2005), Cross-shelf penetrating fronts off the southeast coast of China observed by MODIS, *Geophys. Res. Lett.*, *32*, L19603, doi:10.1029/2005GL023815.

Zavala-Hidalgo, J., S. L. Morey, and J. J. O'Brien (2003), Seasonal circulation on the western shelf of the Gulf of Mexico using a high-resolution numerical model, *J. Geophys. Res.*, *108*(C12), 3389, doi:10.1029/2003JC001879.

Zhang, X., S. F. DiMarco, D. C. Smith IV, M. K. Howard, A. E. Jochens, and R. D. Hetland (2009), Near-resonant ocean response to sea breeze on a stratified continental shelf, *J. Phys. Oceanogr.*, *39*(9), 2137–2155.

Zhang, X., D. C. Smith IV, S. F. DiMarco, and R. D. Hetland (2010), A numerical study of sea-breeze-driven ocean Poincare wave propagation and mixing near the critical latitude, *J. Phys. Oceanogr.*, *40*(1), 48–66.

Zhang, X., M. Marta-Almeida, and R. D. Hetland (2012a), A high-resolution pre-operational forecast model of circulation on the Texas-Louisiana continental shelf and slope, *J. Oper. Oceanogr.*, *5*(1), 19–34.

Zhang, X., R. D. Hetland, M. Marta-Almeida, and S. F. DiMarco (2012b), A numerical investigation of the Mississippi and Atchafalaya freshwater transport, filling and flushing times on the Texas-Louisiana shelf, *J. Geophys. Res.*, doi:10.1029/2012JC008108, in press.